Journal of Pharmaceutical Analysis 8 (2018) 194–201

Contents lists available at ScienceDirect

Journal of Pharmaceutical Analysis

journal homepage: www.elsevier.com/locate/jpa
www.sciencedirect.com

Original Research Article

Physics, chemistry, and Hirshfeld surface analyses of gamma-irradiated thalidomide to evaluate behavior under sterilization doses

Valner A.F.S.N. Mussel [a], Max P. Ferreira [b], Maria B.F. Marques [a], Maria I. Yoshida [a], Mariana R. Almeida [a], Bernardo L. Rodrigues [a], Wagner N. Mussel [a,*]

[a] Departamento de Química, ICEx, Universidade Federal de Minas Gerais - UFMG, Av. Antônio Carlos 6627, 31270-901 Belo Horizonte, MG, Brazil
[b] CNEN-CDTN, Comissão Nacional de Energia Nuclear - Centro de Desenvolvimento da Tecnologia Nuclear, Av. Antônio Carlos, 6627 Belo Horizonte, MG, Brazil

ARTICLE INFO

Article history:
Received 9 June 2017
Received in revised form
24 January 2018
Accepted 25 January 2018
Available online 24 May 2018

Keywords:
Thalidomide
Thermal stability
Polymorphs
Gamma irradiation
Hirshfeld

ABSTRACT

Thalidomide was indicated as a sedative and antiemetic and prescribed for pregnant women. Its tragic teratogenic effects culminated in withdrawal from the market. Since the discovery of its anti-angiogenic and anti-inflammatory actions, thalidomide has been used in the treatment of leprosy and multiple myeloma, which justify studies of its stability. We investigated the effects of irradiation of thalidomide up to 100 kGy (fourfold the usual sterilizing dose for pharmaceutics). The β polymorph of thalidomide was obtained in an isothermal experiment at 270 °C. All samples underwent gamma irradiation for specific times. At different doses, decomposition of the pharmaceutical was not observed up to 100 kGy. The observed effect was angle turning between the phthalimide and glutarimide rings modulated by repulsion towards the carbonyl group, leading to a stable energetic configuration, as measured by the equilibrium in the torsion angle after irradiation. The thalidomide molecule has a center of symmetry, so a full turn starting from 57.3° will lead to an identical molecule. Further irradiation will start the process again. Samples irradiated at 30 and 100 kGy have more compact unit cells and a lower volume, which leads to an increase in the intermolecular hydrogen interaction within the unit cell, resulting in higher thermal stability for polymorph α.

1. Introduction

To ensure adequate conditions of use, sterility is a crucial attribute to any pharmaceutical material, main component, excipient, or formulation. In general, sterilized materials should have microbial survivor probability of $< 10^{-6}$. This criterion is the basis of the sterility assurance level.

There are several sterilization procedures, and each has advantages and disadvantages [1,2]. There is no suitable procedure for general use. Physical removal of microorganisms by membrane filtration does not require heat. Dry heat or even moist heat promotes microbiological reduction at high temperature, but results in considerable degradation of temperature-sensitive materials or devices. Sterilization using ethylene oxide is highly effective but can leave a toxic residue in porous materials such as implants. Electron-beam radiation can be used to prevent temperature effects and toxic residues in the final material, but is limited by poor penetration in bulky materials.

Gamma irradiation has advantages over other conventional sterilization methods in solids: high penetration, uniform efficacy, low isothermal stability, and absence of toxic residues. The main advantage is that irradiation can be used as the final sterilization procedure in starting materials and final products. In this way, the usual 25kGy dose can ensure sterilized pharmaceutical materials [2,3]. Due to the potential sensitivity of pharmaceuticals, validation procedures with lower doses are usually accepted as long as reliable and adequate reduction of the biologic burden can be ensured. In this way, the risk of undesired effects over pharmaceuticals, formulations, or devices submitted to the sterilization process is minimized [4].

Thalidomide ((RS)-2-(2,6-dioxopiperidin-3-il)-1H-isoindol-1,3 (2H)-dione) was synthesized by Chemie Grünenthal in West Germany in 1954. It was introduced to the West German market in 1956 as an antiemetic for pregnant women. In the 1960s, the teratogenic effects of this drug were recognized. Fetal malformation due to the S-isomer of thalidomide resulted in restricted use of thalidomide and increased surveillance by regulatory agencies [5].

Since then, thalidomide has been recognized as having anti-angiogenic and anti-inflammatory properties. It has been used to treat leprosy and multiple myeloma. Hence, stability studies of thalidomide under radioactive stress aimed at sterilization of the drug are warranted [5].

Peer review under responsibility of Xi'an Jiaotong University.
* Corresponding author.
E-mail address: wdmussel@ufmg.br (W.N. Mussel).

https://doi.org/10.1016/j.jpha.2018.01.005
2095-1779/

2. Materials and methods

A sample of thalidomide from a validated production batch was obtained during the shelf-life of this pharmaceutical. All analyses were conducted within the validity period of the batch.

2.1. Powder X-ray diffraction (PXRD)

PXRD data were collected in an XRD-7000 diffractometer (Shimadzu, Kyoto, Japan) at room temperature under 40 kV, 30 mA, using CuK_α ($\lambda = 1.54056$ Å) equipped with polycapillary focusing optics under parallel geometry coupled with a graphite monochromator. The sample was spun at 60 rpm, and scanned over an angular range of 4–60° (2θ) with a step size of 0.01° (2θ) and a time constant of 2s/step. All fitting procedures were obtained using FullProf Suite [6,7]. Crystalexplorer v 17 was used to calculate the Hirshfeld surface [8].

2.2. Single-crystal X-ray diffraction (SCXRD)

SCXRD data were collected in a Gemini A Ultra X-ray Diffraction system (Agilent Technologies, Santa Clara, CA, USA) at room temperature using a MoK_α ($\lambda = 0.71073$ Å) tube as the X-ray source, equipped with a graphite monochromator and a charge-coupled device plate detector. Data collection and refinement details are given in Table 1.

2.3. Thermogravimetric analysis (TGA) and differential thermal analysis (DTA)

TGA and DTA experiments were carried out on a DTG60H system (Shimadzu) in a dynamic N_2 atmosphere (50 mL/min) using alumina pans containing ≈2.0 mg of sample. Experiments were conducted at a heating rate of 10 °C/min from 25 °C to 400 °C.

2.4. Differential scanning calorimetry (DSC)

DSC experiments were undertaken on a DSC60 system (Shimadzu). The equipment cell was calibrated with indium (melting point, 156.6 °C; heat of fusion, $\Delta H_{fus} = 28.54$ J/g) and lead (melting point, 327.5 °C). Aluminum pans containing ≈1 mg of sample were used under a dynamic N_2 atmosphere (50 mL/min) and a heating rate of 10 °C/min from 25 °C to 300 °C. Thalidomide can exist as two polymorphs, α and β, and the latter shows different thermal behavior. Therefore, an isothermal experiment was carried out at 270 °C to obtain a pure material for comparison, as needed.

Table 1
Single crystal refinement data for polymorph α, space group, Hall symbol, lattice parameters *a*, *b* and *c* (Å), ß angle (θ), volume, number of formulae unit per unit cell, X-ray density, wavelength, experimental angular range (θ), crystal absorption coefficient, crystal shape and dimensions, number of reflections considered for cell parameters calculation, and independent reflections used for single crystal fitting.

Crystal data	Values
$C_{13}H_{10}N_2O_4$	Thalidomide
Space group	Monoclinic *P*21/*n*
Hall symbol	-P 2yn
a ± σ (Å)	8.2440 ± 0.0007
b ± σ (Å)	10.0899 ± 0.0009
c ± σ (Å)	14.8991 ± 0.0001
β ± σ (degrees)	102.636 ± 0.008
Volume ($Å^3$)	1209.31 ± 0.02
Z	4
X-ray density (Dx)	1.418 mg/m^3
Wavelength (Mo/Kα)	0.71073 Å
Experimental angular range (θ)	3.2–26.8°
Crystal absorption coefficient (μ)	0.11 mm^{-1}
Crystal shape and dimensions	Prism, 0.24 mm × 0.24 mm × 0.80 mm
Number of reflections considered for cell parameters calculation	1449
Independent reflections used for single crystal fitting	2884

2.5. Ultraviolet spectroscopy

Ultraviolet spectroscopy was undertaken at 200–400 nm for thalidomide at 10 μg/mL in ethanol on a spectrophotometer (1800; Shimadzu). Origin v9.1 was used to adjust data.

2.6. Raman spectroscopy

Raman spectroscopy of solid thalidomide was done on a confocal micro-Raman spectrometer (Senterra; Bruker, Billerica, MA, USA) with an excitation laser set at 785 nm. The measurement conditions were as follows: integration time of 5 s; spectral resolution of 3–5 cm^{-1}; and spectral range of 2000–100 cm^{-1}. The laser was focused with a 4× dry objective lens, with the laser power set to 25 mW. Origin v9.1 was used to adjust data.

2.7. Gamma irradiation

Experiments involving gamma irradiation were done at Comissão Nacional de Energia Nuclear-Centro de Desenvolvimento da Tecnologia Nuclear (Belo Horizonte, MG, Brasil). The radiation system (IR-214; MDS Nordion, Ottawa, Canada) was equipped with a dry cobalt-60 source. The source had a maximum activity of 2200 TBq (60,000 Ci). The specific irradiation times were calculated, and then all samples were exposed to doses of 2, 5, 10, 15, 25, 30 or 100 kGy.

2.8. Attenuated total reflection Fourier transformed infrared spectroscopy (ATR-FTIR)

FTIR analysis was performed at room temperature on a Spectrum 1000 spectrophotometer (PerkinElmer, United States) equipped with an attenuated total reflectance (ATR) accessory. The sample was pressed into a zinc selenide crystal, and 32 scans were averaged. For single FTIR without ATR, the samples were measured in KBr pressed pellets in the wavenumber range between 400 and 3400 cm^{-1} at room temperature, with a resolution of 4 cm^{-1}.

2.9. Statistical analyses

Data are the mean ± standard deviation. All fitting procedures took into account three independent measurements with statistical analyses conducted using Origin v9.1.

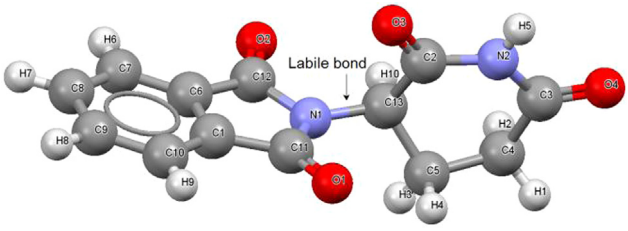

Fig. 1. Thalidomide molecule showing the labile bond between phthalimide and glutarimide rings.

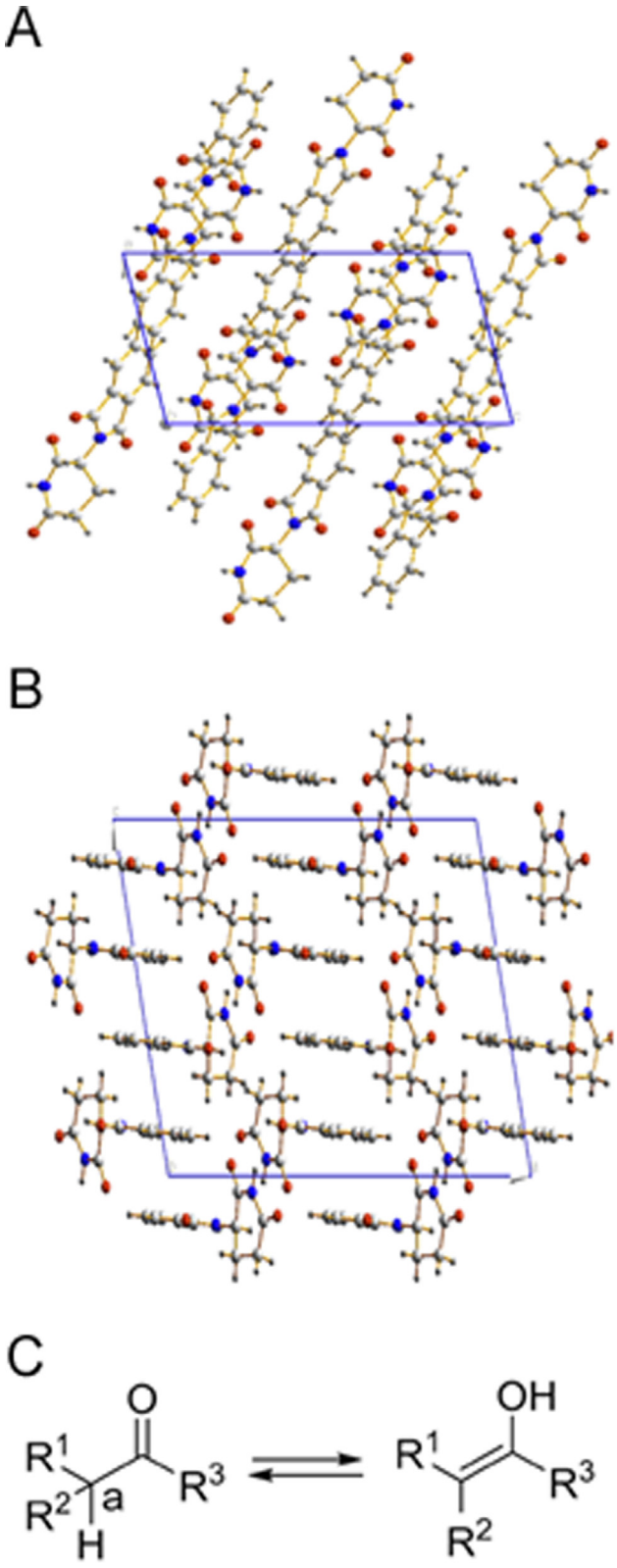

Fig. 2. The crystal structure of the polymorphs α (A) (a = 8.233(1) Å, b = 10.070(2) Å, c = 14.865(2) Å, α = γ = 90.0° and β = 102.53(2)°, monoclinic, P 21/n, Z = 4) and β (B) (a = 20.679(5) Å, b = 8.042(2) Å, c = 14.162(5) Å, α = γ = 90.0° and β = 102.86(3)°, monoclinic, C 2/c, Z = 8), and (C) keto-enol tautomerization.

3. Results and discussion

The thalidomide molecule has a labile bond that can be turned around from phthalimide and glutarimide rings (Fig. 1).

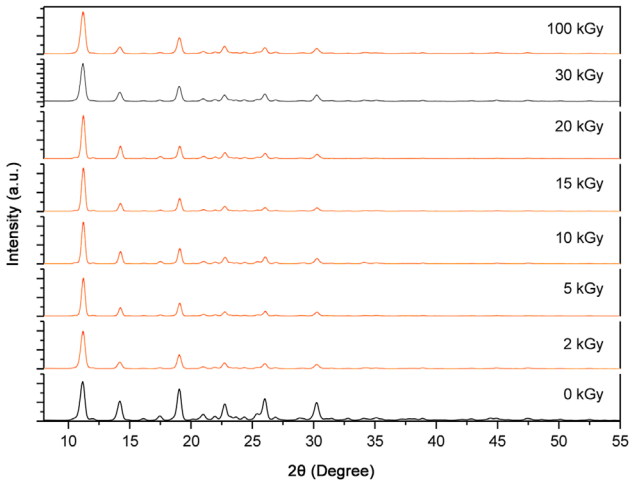

Fig. 3. Powder X-ray diffraction experiments for irradiated thalidomide samples for 0, 2, 5, 10, 15, 20, 30 and 100 kGy. All samples were irradiated under the same conditions, only different times.

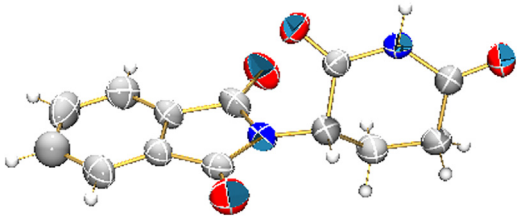

Fig. 4. Crystal projection of the asymmetric unit. Carbon (grey), oxygen (red) and nitrogen (blue) atoms. ORTEP plotted ellipsoids with 50% probability.

In the thalidomide chemical structure, the chiral center has a neighboring ketone that may undergo to the enol form, then re-forming it when switching back to the keto form. Even with uptaking of the correct R-thalidomide, a keto-enol tautomerization happened inside the human body, it would racemase into a mixture of R,S-thalidomide and the corresponding enol forms. The S-thalidomide causes the birth defects (Fig. 2).

The intensity of a diffracted peak of a certain reflection (*hkl*) plane for a given chemical structure is a direct contribution of the structural factor, which in turn corresponds to the number of electrons diffracting the X-ray beam on that plane. If any plane in the structure reduces its number of electrons, a direct effect of that condition will be a decrease in the intensity of that specific plane, and the resulting system will be a plane with lower electron density. In the solid state, the atoms in a structure are much less labile than in solubilized material because of numerous mutual interactions (e.g., Van der Waals forces and/or hydrogen bonding). The fitting procedure was designed to allow the torsion angle between phthalimide and glutarimide rings to vary freely within the extraction and adjustment of the intensities in the diffraction.

The thalidomide structure $C_{13}H_{10}N_2O_4$ space group $P21/n$ has a torsion angle of 57.28° (2θ). This structure was taken as a reference, with all procedures starting from the same template molecule, by varying the fitting sequence as follows: (i) parameterization of the background with five polynomial terms; (ii) U, V and W (FWHM) of the pseudo-Voight function; (iii) profile parameters NA and NB of the pseudo-Voight function; (iv) asymmetry factors P1, P2, P3 and P4 of the Berar–Baldinozzi asymmetric correction; (v) a and b beyond the beta angle of the crystal lattice; (vi) torsion angles N1-C11-C13-C2 with the initial

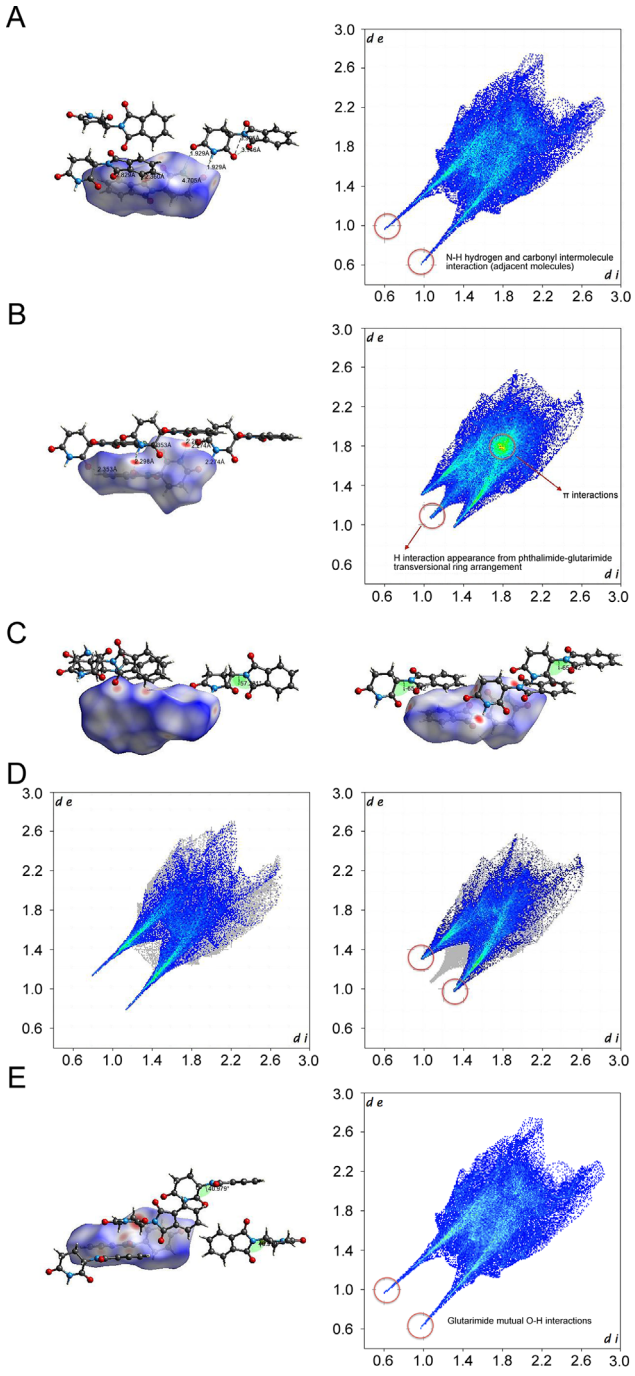

Fig. 5. Hirshfeld surface analysis and corresponding overall fingerprints for polymorphs α and β (A and B, respectively), the torsion angles (C), the fingerprint O-O interactions (π- π respectively) (D). The 2 kGy irradiated α polymorph with respectively torsion angle and overall fingerprint (E).

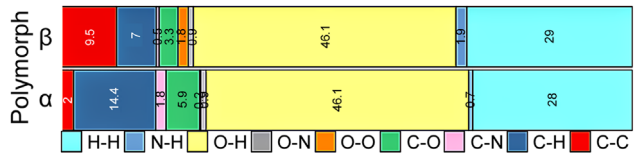

Fig. 6. Hirshfeld surface analysis and overall contributions for all atoms pairs in polymorphs α and β.

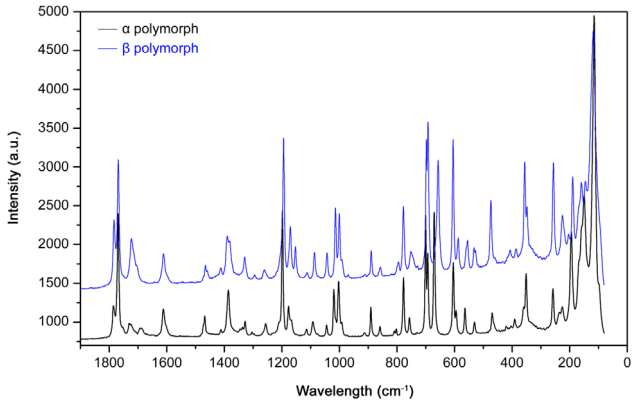

Fig. 7. Raman experimental spectra of polymorphs α and β evidencing the spectra differences.

value set to 57.28° (2θ); (vii) isotropic thermal parameter functions for all atoms. Fig. 3 shows the experimental XRD pattern for all doses.

SCXRD was carried out on a recrystallized sample from an original polymorph α sample by solvent evaporation. To 20 mL of a methanol: water (5:3) solution was added 25 mg of polymorph α, which resulted in a supersaturated solution. Non-solubilized crystals were filtered out, and the solution was allowed to stand to recrystallize over 23 days. The crystal data, collection, and details of structure refinement of polymorph α are summarized in Table 1. Refinement was carried out in the absence of anomalous scattering. Changes in illuminated volume were kept to a minimum, and were taken into account [9–14] using multi-scan inter-frame scaling. Hydrogen atoms were geometrically fixed to their bonded atoms, with their thermal isotropic term, $U_{iso}(H)$ in the range 1.2–1.5 times U_{eq} of the parent atom, after which the positions were refined with adequate constraints. Fig. 4 shows the asymmetric unit as an Ortep plot for the determination of crystal structure, as well as the unit cell ellipsoids with 50% probability.

Hirschfeld surface analyses can provide a deep understanding of certain characteristics based on electron distribution, π interactions, and the contributions of pairs of atoms. Polymorphs α and β showed substantial differences for each fingerprint (Figs. 5A and B). Polymorph β showed a relatively large π interaction on the phthalimide ring. This was a direct evaluation of close contact and the internal distribution of the β cell lattice (Fig. 5B). A large

Table 2
Torsion angle (degrees θ), lattice parameters (Å), β (degrees θ) and Rp goodness of fitting parameter (%).

Dose (kGy)	Torsion angle (degrees θ)	$a \pm \sigma$ (Å)	$b \pm \sigma$ (Å)	$c \pm \sigma$ (Å)	β ± σ (degrees θ)	Rp (%)
0	57.3 ± 0.1	8.233 ± 0.001	10.070 ± 0.002	14.865 ± 0.002	102.53 ± 0.02	*
2	40.1 ± 0.2	8.154 ± 0.004	9.950 ± 0.004	14.714 ± 0.005	102.68 ± 0.02	0.1215
5	41.0 ± 0.1	8.168 ± 0.002	9.976 ± 0.003	14.769 ± 0.004	102.79 ± 0.02	0.1351
10	47.4 ± 0.1	8.251 ± 0.002	10.063 ± 0.002	14.892 ± 0.003	102.86 ± 0.02	0.1020
15	45.0 ± 0.2	8.171 ± 0.001	9.975 ± 0.002	14.754 ± 0.003	102.82 ± 0.02	0.0919
20	47.0 ± 0.1	8.143 ± 0.003	9.943 ± 0.003	14.708 ± 0.004	102.68 ± 0.02	0.1048
30	44.4 ± 0.5	8.204 ± 0.004	9.957 ± 0.004	14.825 ± 0.006	102.79 ± 0.03	0.1400
100	40.2 ± 0.1	8.146 ± 0.004	9.944 ± 0.004	14.717 ± 0.005	102.70 ± 0.02	0.1380

Table 3
Experimental and calculated Raman's observed peak, fully assigned for α polymorph.

Experimental (cm^{-1})	Calculated (cm^{-1})	Observed structure assignments
1785	1896	Symmetrical stretching C═O
1769	1882	Symmetrical stretching C═O
1754	1854	Symmetrical stretching C═O
	1839	Asymmetric stretching C═O
1730	1722	Ring stretch
1688	1686	Ring stretch
	1496	Symmetrical deformation CH_2
	1493	Ring stretch C-C
1468	1466	Ring symmetrical stretching C-N-C
	1449	Ring symmetrical stretching C-N-C
	1424	Ring symmetrical stretching C-N-C, CH
1412	1417	Ring symmetrical stretching C-N-C, C-H
1386	1402	Ring deformation, asymmetrical stretching C-N-C, C-H
1327	1315	Asymmetrical stretching C-N-C, deformation C-H
1256	1235	Ring strain C-N
1210	1214	Strain C-C
1198	1193	Ring deformation, stretching C-C═O
1176	1178	Ring deformation, stretching CH_2-CH_2-CH
1166	1167	Ring deformation, stretching CH_2-CH_2-CH
	1155	Asymmetric stretching CH_2
1114	1127	Ring stretching CH, CH_2
1092	1070	Asymmetric deformation CH_2 stretching CH_2-C═O
1045	1040	Ring stretching, C-N-R_2
1019	1010	Ring stretching, asymmetric stretching CH
1003	986	Ring stretching, symmetric stretching CH
	955	Symmetric deformation CH_2, CH_2-C═O
	935	Ring asymmetric stretching CH
913	911	Deformation CH_2, CH
891	919	Ring symmetric stretching CH
859	848	Ring deformation, ring symmetric stretching CH
809	804	Ring deformation, ring asymmetric stretching CH
802	799	Asymmetric ring deformation
	756	Symmetric stretching C-N-C
757	729	Ring stretching, asymmetric stretching CH_2
701	697	Out of plane ring deformation
693	694	Ring deformation CH, CH_2
671	670	Ring symmetric stretching CH
	665	Ring deformation CH, CH_2
604	641	Ring deformation, stretching CH, CH_2
595	585	Ring deformation CH, CH_2
564	551	Ring symmetric stretching CH, ring deformation
	541	Ring out of plane deformation
531	529	Ring out of plane deformation
	506	Ring stretching CH, CH_2
	495	Ring asymmetric deformation CH
469	472	Deformation C-C═O
404	408	Out of plane deformation C-N-C, deformation CH_2
391	365	Out of plane deformation C-N-C
360	359	Deformation CH_2
351	344	Asymmetric deformation C═O, CH_2
258	262	Asymmetric deformation CH_2
236	243	Out of plane ring deformation
225	240	Out of plane ring deformation
	222	Ring deformation
194	205	Asymmetric deformation CH_2

distance of approximately 1.1 Å from the inside surface (*di*) interaction on polymorph β was related to the appearance of hydrogen-atom interaction from the phthalimide–glutarimide transversional ring arrangement within the unit cell (Figs. 5B and C). The two

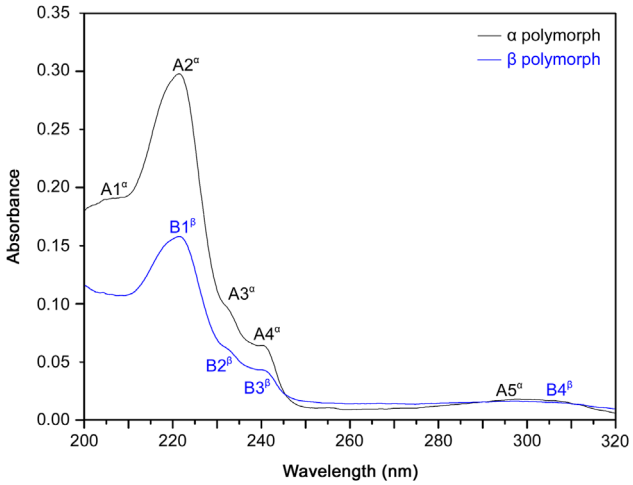

Fig. 8. UV experimental spectra for α and β polymorphs.

interactions at about 1.0 and 1.3 Å (Fig. 5B) from the inside surface (*di*) were due to the glutarimide–glutarimide nitrogen-hydrogen and carbonyl group of two close molecules within the unit cell. The overall O-H interactions showed shorter distances from the inside surface (*di*) of about 1.0 and 1.3 Å for α and β, respectively, and showed a more compact unit cell for polymorph β (Fig. 5D). For polymorph α irradiated at 2 kGy, the two adjacent glutarimide rings within the unit cell were responsible for the mutual O-H interactions leading to hydrogen-bond formation and/or the possibility of a tautomeric pair structure (Fig. 5E). Fig. 6 shows the individual contribution from each atom pair to the overall probability of interaction over the thalidomide molecule [15–17].

Raman spectroscopy was undertaken for both polymorphic forms of thalidomide. Theoretical calculations were carried out to increase understanding of the observed vibrational modes. Theoretical calculations were done using the structures of each polymorph published by the Cambridge Crystallographic Data Center (Cambridge, UK) using Spartan v14. Fig. 7 shows the experimental Raman spectra for polymorphs α and β.

Table 2 shows the experimental and theoretical bands (as assigned) for each mode of polymorph α. For symmetric stretching of the carbonyl group, centered at 1785 and 1769 cm^{-1}, no equivalent vibrational modes, when compared with polymorph β, were identified.

Asymmetric stretching of the carbonyl group was identified at 1754 cm^{-1}. Vibrational modes appeared at two carbonyl groups for polymorph α whereas, in polymorph β, such modes were related primarily only to one carbonyl group. The stretching region of the CH_2-CH bond in the glutarimide ring showed peaks at 1166 and 1176 cm^{-1}, and showed a substantial difference for the ratio and axial offset for the two polymorphs. Peaks on the spectrum for polymorph α at 701 and 693 cm^{-1} were assigned to the vibrational modes corresponding to ring deformations outside the plane. Peaks at 604 and 595 cm^{-1} were assigned to the ring deformation and stretching of the CH group and CH bonds. For deformation out of the plane, peaks at 404, 391, 236 and 225 cm^{-1} were observed. For crystalline structures in different polymorphs, the vibrational modes in the low vibrational frequency region ($< 200\ cm^{-1}$) are attributed to vibrations of the crystal lattice, and that region can be regarded as a "second fingerprint" of the Raman spectrum for each substance (Table 3) [18,19]. Comparison of these data suggested that differences in the spectra of polymorphs α and β were due to compression of their molecules and the way they were interacting in their crystal lattices; these effects influenced

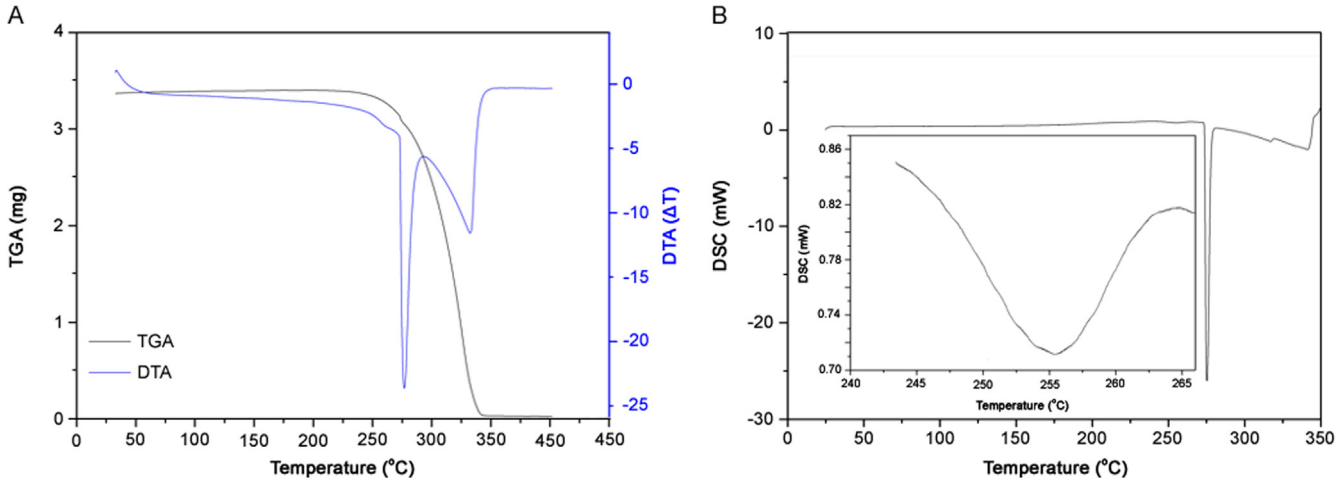

Fig. 9. (A) TGA/DTA simultaneous curve of α polymorph form; (B) DSC curve of α polymorph form, with inset zoom of the endothermic peak.

their vibrational modes directly. Transformation between thalidomide polymorphs was achieved by providing adequate energy for the crystalline lattice with the aim of reorganization. This procedure was accompanied by TGA, DTA and DSC.

In simultaneous TGA/DTA, mass loss was observed only once at an onset temperature of 264 °C, suggesting that the material was anhydrous and pure. The DTA curve revealed two endothermic peaks corresponding to fusion of polymorphs α and β, respectively. The DSC curve showed two endothermic events at onset temperatures of 245 °C and 274 °C. Fig. 8 shows the UV spectra for polymorphs α and β. We observed five bands for polymorph α (A1, A2, A3, A4 and A5) and four bands for polymorph β (B1, B2, B3 and B4). The A1 band at 207 nm is related to the n → π* transitions in aromatic compounds. The A2 and B1 bands at 221 nm and 222 nm, respectively, are related to π* conjugated systems, showing aromatic compounds to have chromophore substitution. The A3 and B2 bands at 232 nm and 233 nm, respectively, are related to tautomers generated by the working pH of the solution. The A4 and B3 bands at 240 nm and 241 nm, respectively, are the characteristic bands of thalidomide. The A5 and B4 bands both at 300 nm are related to groups with a low-energy configuration state, just like the carbonyl groups in thalidomide. For better visualization of the first endothermic peak, enlargement of this region in the curve is shown (Fig. 9). This event was identified as a crystalline transition between the two polymorphs of thalidomide.

The second endothermic event corresponded to decomposition of the formed material, with this being only the β form in the case of total conversion and a mixture of α and β in the case of partial conversion [19]. To confirm these occurrences, an isotherm at 270 °C using the material for further powder XRD was undertaken (Fig. 10). Comparison of the diffractograms and interplanar distances enabled us to confirm and identify the material as polymorph β.

We wished to visualize possible changes in thermal behavior of the material after irradiation. Hence, DSC was done with samples receiving doses of 2, 5, 30 or 100 kGy. In the DSC curve of the samples irradiated with 2 and 5 kGy, a single endothermic peak with an onset temperature of 275 °C was noted for both samples. This finding suggested total conversion of the α form into the β form during heating, so this peak was designated as the fusion follow by decomposition of polymorph β (Fig. 11). The DSC curves of samples irradiated with 30 and 100 kGy revealed two endothermic peaks with onset temperatures of 272 °C and 275 °C for samples irradiated with 30 kGy and at 272 °C and 274 °C for samples irradiated with 100 kGy (Fig. 12).

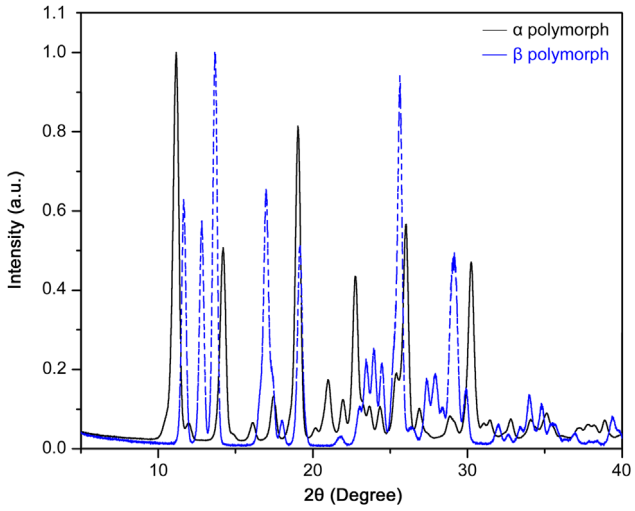

Fig. 10. Comparative diffractogram between α and β polymorphs.

We designated the first peak as the fusion of polymorph α and the second peak as the fusion of polymorph β for both curves. Different from the report by Reepmeyer and colleagues [14], the DSC curve in our study was carried out at a heating rate of 10 °C/min, but we observed values very close to those reported by Reepmeyer and colleagues. We propose that after irradiation with doses of 30 and 100 kGy, polymorph α acquired higher thermal stability in relation to polymorphic transformation. Therefore, the fusion and decomposition temperature of α form was visualized in DSC curves instead of its crystalline transformation, as shown in the physicochemical characterization of the material. The irradiated sample had a more compact unit cell, so there was an increase in hydrogen-atom interactions within the unit cell, resulting in an increase in thermal stability of polymorph α.

4. Conclusion

The observed turning around phthalimide and glutarimide rings already occurs at low radiation values (e.g., 2 kGy). Eventually, the absorbed energy will overcome the repulsive force due to the proximity of the carboxyl group and produce a full turn. With a continuous supply of energy, the system rotates completely at

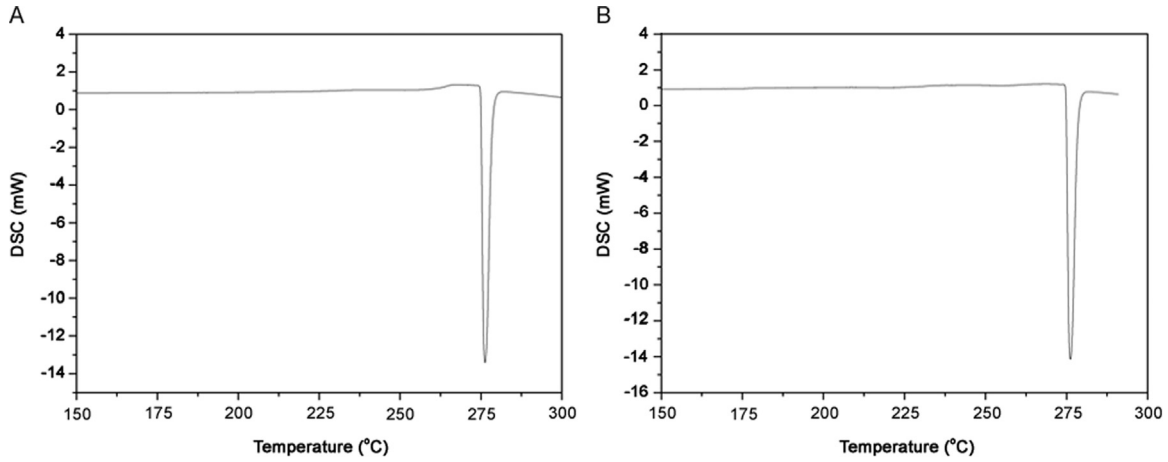

Fig. 11. DSC curves of α polymorph form after (A) 2 kGy dose and (B) 5 kGy dose.

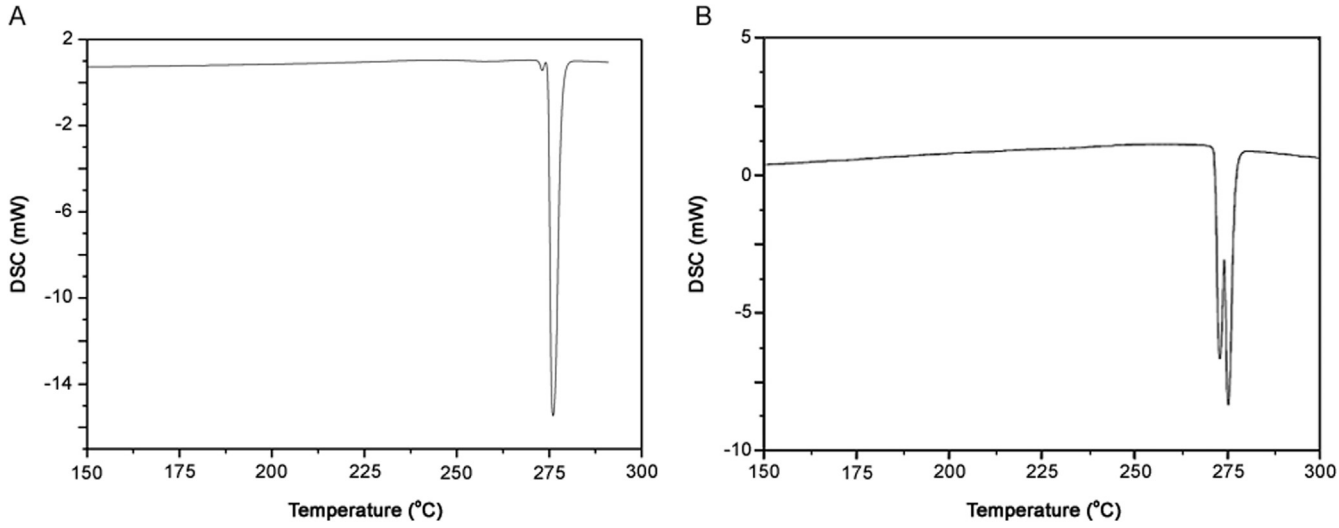

Fig. 12. DSC curves of α polymorph form after (A) 30 kGy dose and (B) 100 kGy dose.

higher doses of 15, 20, 30 and 100 kGy. With higher doses, the full turning effect is reached, allowing the network to relax its tension. The thalidomide molecule has a center of symmetry. Therefore, one full turn of phthalimide and glutarimide rings between each other, starting from 57.3 °, will lead to the same molecule, with stabilization of the final angle based on the total amount of absorbed energy. After a full turn, the process starts again. Irradiated samples at 30 and 100 kGy had more compact unit cells and a lower volume, so there was an increase in the intermolecular interaction between hydrogen atoms within the unit cell, which resulted in higher thermal stability for polymorph α. At 30 and 100 kGy, each melting point could be seen separately, which was a different situation compared with that of the non-irradiated sample. A fourfold increase in the usual dose used in pharmaceuticals is employed for gamma-ray sterilization. Thalidomide molecules can release excess energy by turning the bond between phthalimide and glutarimide rings. Hence, gamma-ray sterilization of pure thalidomide before use in fixed-dose pharmaceutical formulations is possible.

Conflicts of interest

The authors declare that there are no conflicts of interest.

Acknowledgments

The authors would like to thank the CNEN-CDTN (Comissão Nacional de Energia Nuclear – Centro de Desenvolvimento da Tecnologia Nuclear) LIG (Laboratório de Irradiação Gama) facility for the assistance, and Fundação de Amparo à Pesquisa do Estado de Minas Gerais (FAPEMIG) (APQ-02087-14), Conselho Nacional de Desenvolvimento Científico e Tecnológico (CNPq) (245914/2012), Coordenação de Aperfeiçoamento de Pessoal de Nível Superior (CAPES) (PNPD-N-1648694 - scholarship Nº 2016752283) and Pró-Reitoria de Pesquisa/UFMG for financial support.

References

[1] Health Products and Food Branch Inspectorate: Process Validation: Terminal Sterilization Processes for Pharmaceutical Products, Supersedes: GUI-0007, GUI-0009 and GUI-0010, (GUIDE-0074), OTTAWA, Ontario, Canada, 2006.
[2] EN ISO 13408-1:2008(en), Aseptic processing of health care products—Part 1: General requirements, compilation prepared by Online Browsing Platform (OBP), 2008, 〈https://www.iso.org/obp/ui/#iso:std:iso:13408:-1:ed-2:v1:en〉.
[3] AAMI/ISO 11137-2:2013, Sterilization of health care products - Radiation - Part 2: Establishing the sterilization dose (revision of 11137-2: 2012), ISBN(s): 1570205027, 2013.
[4] J. Agalloco, USP Microbiology & Sterility Assurance, Expert Committee USP: Activities Impacting Sterilization & Sterility Assurance, USP 35 1211, revision 2008.

[5] F. Hasanain, K. Guenther, W.M. Mullett, et al., Gamma sterilization of pharmaceuticals - a review of the irradiation of excipients, active pharmaceutical ingredients and final drug product formulations, J. Pharm. Sci. Technol. 68 (2014) 113–137.
[6] T. Roisnel, J. Rodriguez-Carvajal, WinPLOTR: a Windows tool for powder diffraction patterns analysis Materials Science Forum, Proceedings of the Seventh European Powder Diffraction Conference, EPDIC 7, 2000:118–123.
[7] J. Rodriguez-Carvajal, T. Roisnel, FullProf. 98 and WinPLOTR: new windows 95/NT applications for diffraction. Commission for powder, Int. Union Crystallogr. Newsl. 20 (1998) 35.
[8] M.J. Turner, J.J. McKinnon, S.K. Wolff, et al., CrystalExplorer17, University of Western, Australia, 2017 ⟨http://crystalexplorer.scb.uwa.edu.au⟩.
[9] C.H. Görbitz, What is the best crystal size for collection of X-ray data? Refinement of the structure of glycyl-L-serine based on data from a very large crystal, Acta Cryst. B55 (1999) 1090–1098.
[10] R.I. Cooper, A.L. Thompson, D.J. Watkin, CRYSTALS enhancements: dealing with hydrogen atoms in refinement, J. Appl. Cryst. 43 (2010) 1100–1107.
[11] G.M. Sheldrick, A short history of SHELX, Acta Cryst. A64 (2008) 112–122.
[12] P.W. Betteridge, J.R. Carruthers, R.I. Cooper, et al., CRYSTALS Version 12: software for guided crystal structure analysis, J. Appl. Cryst. 36 (2003) 1487.
[13] D.J. Watkin, C.K. Prout, J.R. Carruthers, et al., Crystals Issue 10, Chemical CrystallographyLaboratory, Oxford, UK, 1996.
[14] J.C. Reepmeyer, M.O. Rhodes, D.C. Cox, et al., Characterization and crystal structure of two polymorphic forms of racemic thalidomide, J. Chem. Soc. Perkin Trans. 2 (9) (1994) 2063–2067.
[15] M.A. Spackman, D. Jayatilaka, Hirshfeld surface analysis, CrystEngComm 11 (2009) 19–32.
[16] M.A. Spackman, J.J. McKinnon, Fingerprinting intermolecular interactions in molecular crystals, CrystEngComm 4 (2002) 378–392.
[17] M.J. Turner, J.J. McKinnon, D. Jayatilaka, et al., Visualisation and characterisation of voids in crystalline materials, CrystEngComm 13 (2011) 1804–1813.
[18] P.J. Larking, M. Dabros, B. Sarsfield, et al., Polymorph characterization of active pharmaceutical ingredients (APIs) using low-frequency Raman spectroscopy, Appl. Spectrosc. 68 (7) (2014) 758–776.
[19] E.P.J. Parrot, B.M. Fischer, L.F. Fladden, et al., Terahertz spectroscopy of crystalline and non-crystalline solids, Terahertz spectroscopy and imaging Springer Series in Optical Sciences book series (SSOS), 171, 2012:191–227.